Ultra Scientist Vol. 24(3)B, 445-451 (2012).

Investigations of the alloy hardening among the Zinc-Beryllium-Selenide ternary solid solutions by using Extended x-ray absorption fine structure (EXAFS) technique

SHABINA KHAN[a1], PANKAJA SINGH[1], JAVED MAZHER[2]
and NARAYAN BEHERA[3]

(Acceptance Date 15th Octoberber, 2012)

Abstract

A detailed ab initio analysis is carried out for the cationic substitution doped mixed alloy's theoretical EXAFS simulations. Suitable data processing codes are used for the subsequent experimental EXAFS spectral fittings. We have simulated various x-ray scattering single and multiple paths around the core atomic environ and subsequently they are compared with the spectroscopic results. As-obtained parametric values are used to find the hardening and crystalline disorders among these heavily Be doped ZnSe ternaries. The hardening phenomenon amongst the alloys are explained by using the doping related variations of the Zn-Se and Be-Se bond lengths and the presence of structural stabilities during the initial stages of alloying.

Key words: Mixed Alloys, EXAFS, doping and Solid solution hardening.

1. Introduction

The $Zn_{1-x}Be_xSe$ alloys are a new class of II-VI ternary semiconducting compounds that are formed from the binaries with highly contrasting bond length- properties[1]. Previously, fundamental defects in as grown ZnBeSe materials are studied with a positron spectroscopy and the defects responsible for the photoluminescence decay among the compositionally assorted samples are identified in detail[2]. It is found that the alloy exhibits an unusually large contrast in physical properties manifesting in bond stiffness and bond lengths distribution of its constituting bonds, leading to a uniquely well-resolved 1–bond→2–mode behavior as already

reported in the Raman spectra of this system[3]. From such studies it is well established that various defect dissemination mechanisms in ZnSe are significantly reduced on increasing the lattice rigidity and for the reason that high degree of covalent bonding of Be chalcogenides can lead to an increase of shear modulus in such ternaries[4,5]. From Mazher *et. al.*'s previous studies[6,7] on the high-pressure EXAFS, we lead to a verdict of pressure dependence of nearest and next nearest neighbor distances of Zn (or Be) and Se atoms and pseudo Debye–Waller factors σ^2 on such binary and ternary systems. However, factors that determine the dependence of these parameters as a function of the alloy composition are mostly unidentified. At this point it is highly desirable to present our groundwork results of the extended x-ray absorption fine structure (EXAFS) measurements at Zn K edges on the compositionally varied (Zn,Be) Se alloyed samples in ambient conditions at a room pressure to get a better insight into the type of disorders and bond deformations both qualitatively and quantitatively.

2. *Experimental and Theoretical Methods:*

A set of compositionally vibrant six high quality samples (ZnSe, A, B, C, D, and E) of the alloy of $Zn_{1-x}Be_xSe$ are prepared by a high pressure horizontal Bridgman technique with Be cationic mass fraction (x) values of 0.00, 0.06, 0.16, 0.27, 0.33, and 0.42 respectively, details of synthesis method are given elsewhere[8-10]. All the samples are found to acquire ZnS or zinc-blende type of crystal structure. A powdered mixture of ZnSe of purity ~99.999% and beryllium of purity ~99.8% is used as a crucible charge and the temperature of the heating zone is stabilized to 1850 K. The crucible is moved out of the heating zone at the rate of about 2.4 mm/h. At the high temperatures, the beryllium atoms are found to be partially substituting at Zn locations in the host ZnSe lattice and thus we have obtained true $Zn_{1-x}Be_xSe$ solid solutions. Ambient condition EXAFS experiments are performed on the XAS beamline at atmospheric pressure and room temperature. The XAS beamline facilitates the dispersive EXAFS and commissioned at the SOLEIL synchrotron radiation facility located at Gif sur Yvette, France[11,12]. Open source EXAFS analyses code IFEFFIT version 0.102.10 [13] is used for the theoretical fitting of the EXAFS k-oscillations and their FTs. An evenly spaced k- grid (0.05Å^{-1}) is used for fitting the oscillations along with the polarization, local field and core-hole corrections. The fixed data ranges are 3Å^{-1}-15Å^{-1} and 1Å-6 Å for the processed k-oscillations and their FTs respectively. The EXAFS fitting parameters are debye-waller factor σ^2, change in the radial distances from the core Zn atom (ΔL), amplitude correction factor S_o^2, absorption edge energy shift Eo from the theoretical value of the edge (9.562 keV), and also we have increased the second shell beryllium related path degeneracies with increasing values of 'x'.

3. Results and Discussion

The EXAFS technique provides information on the atomic structure around any specific atom, which is the Zn core atom in our experiments[14]. Besides, the Zn core's K edge EXAFS contains information about its near-neighbor atom distances and fluctuations in the corresponding binary or ternary bond lengths.

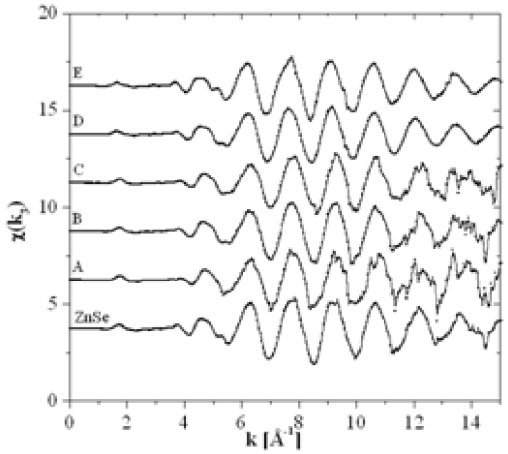

Figure 1. The Zn K edge EXAFS absorption [$\chi(k_3)$] for the $Zn_{1-x}Be_xSe$ samples (A to E) plotted in k–space along with a pure ZnSe spectra. The spectra are arranged vertically upward in increasing order of the Be concentrations and the bottommost is the ZnSe EXAFS.

During analyses, the EXAFS data is first converted from the $\chi(\mu)$ form to the $\chi(k)$ by using the relation, $\delta k = \delta E / 3.9038\sqrt{E - E_0}$. In a figure 1, the EXAFS spectra in k–space for the samples (A to E) are shown after applying k-weighing by multiplying with a factor kS (S, being 1, 2, 3,...). The kS multiplication gives more uniformly distributed EXAFS over the given data range along with the suppression of the larger amplitude oscillations from dominating the smaller ones. The frequency dependence of the amplitude, which is also demonstrated from the EXAFS equation, is given by, $\chi(k) = [\mu(k) - \mu_0(k)] / \mu_0(k) = \sum_j \left(N_j / kR_j^2\right) A_j(k) \sin\left[2kR_j + \psi_j(k)\right]$. Where, N_j is the number of atoms at distance R_j in an atomic shell (j), $\chi(k)$ is an oscillatory component of the absorption after subtracting out a smoothly varying atomic contribution $\mu_0(k)$ and A(k) is the amplitude factor that can be further broken down to give a relation $A_j(k) \propto |f_j(k,\pi)| \exp(-2\sigma^2 k^2) \exp(-2R_j/\lambda)$. Furthermore, the $f_j(k, \pi)$ is the atomic backscattering factor for the photoelectron with wave number k and it depends on the atomic number of the scatterer. Moreover, the EXAFS Debye–Waller factor of $\exp(-2\sigma^2k^2)$ describes the degree of randomness of the sample crystallinity, where σ^2 is the mean squared variation of the radial positions of the atoms about their average due to either structural disorder or thermal vibration. Naturally, the overall amplitude of the fine structure of a particular shell enhances corresponding to the higher coordination (N) and at small distances (R) from the absorbing atom. Typically, we have found a $1/R^2$ type of spherical wave decay in the amplitude maximum with the inter shell distances. Besides, there is also slowly varying photon energy dependence (~1/k)[16,17].

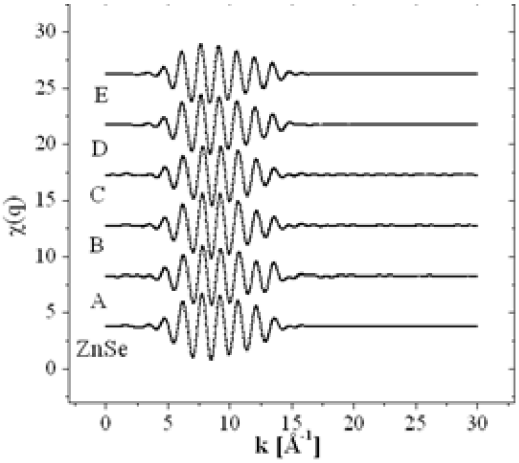

Figure 2. Absorption oscillatory variations [$\chi(q_3)$] for first shell contributions from Zn K edge EXAFS that are plotted in k–space for $Zn_{1-x}Be_xSe$ samples of composition (x) values of 0.0, 0.06, 0.16, 0.27, 0.33 and 0.42. The oscillations are extracted by the first shell window filters and k3-weighted back-FTs.

After filtering, the back FT is performed to give the EXAFS oscillatory part corresponding to the first shell as shown in a figure 2. The only difference between k and q spaces is that the momentum-space is limited in the latter. From the figure 2, note the absence of all higher frequency variations and noise because the contributions from the second and subsequent higher shells are completely removed. It is clear that major contributions in the ZnBeSe's EXAFS oscillation arise only from the first shell.

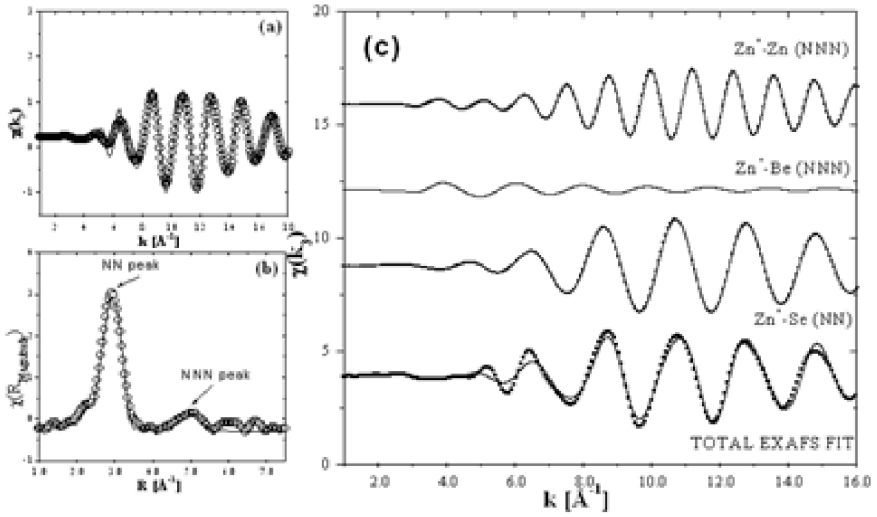

Figure 3. (a) The total IFEFFIT fitting of the Zn K edge EXAFS absorption data for $Zn_{1-x}Be_xSe$ for sample (A) plotted in k-space, $\chi(k_3)$. (b) Total IFEFFIT fitting of Zn K edge EXAFS absorption data for the sample plotted in real-space $\chi(r)$ amplitude radial distributions, which are clearly discernible for first and second shell scattering paths. (c) Extracted oscillatory contributions of different NN & NNN scattering paths from the Zn K edge EXAFS absorption plotted in the k-space.

In figure 3(a), the EXAFS fit is plotted as a smooth runner against the experimental data points (encircled) for sample (A). The fitting path parameters carries the information of change in the path distances L and their average distributions (crystal disorder parameter). As we know, the EXAFS path is the photoelectron scattering distance from the near neighbor (NN) and next nearest neighbor (NNN) atoms before returning to the central atom. The total EXAFS is then just a sum of these individual paths. Using IFEFFIT, we have calculated the single scattering NN and NNN path distances for the atomic co-ordination shells. The theoretical curve plotted as continuous runner in the figures 3(a) & (b) show the perfect overlap of the experimental EXAFS oscillation with the tetrahedrally symmetrical $Zn_{1-x}Be_xSe$ system with that of its IFEFFIT theory having high values of the goodness of fit. We have carried the similar analysis for the different compositions with the value of x changes from 0.06 to 0.42

in the data set undertaken for analysis. The figure 3(c) shows the single scattering paths for NN and NNN co-ordinations and the oscillations [$\chi(q)$] are plotted in the q-space. The top two spectra of figure 3(c) are the back FTs of the second shell corresponding to the NNN distances from the Zn and Be atomic co-ordinations. A collective effect of the second shell atoms is also clearly visible in the form of the second NNN peak of figure 3(b). The lowest spectrum in the figure 3(c) corresponds to the best theoretical fit with the experimental data. The change in single scattering NN distance at the Zn K edge in $Zn_{1-x}Be_xSe$ system roughly corresponds to the change in the bond length (Zn-Se) and depicted by the first peak in the figure 3(b). By making a comparison between these two NNN spectra it is evident that the contribution from the Zn coordination is much greater to that of Be coordination, which is obvious because of the heaviness of Zn atom and the less concentration of Be in this sample, which is only x=0.06. Also the χ -intensities of the Zn*–Be (NNN) is much smaller as compared to that of the Zn*–Zn. Besides it is clear from the upper two spectra of the figure 3(c), the k–space oscillation maxima shifted in Zn*–Be scattering path to the left hand side in comparison to the NNN distance position of the Zn–Zn scattering path. This fact implicates the smaller values of Be–Se bond lengths in contrast to that of Zn–Se bond lengths. Hence in this mixed crystal, we have observed two modes in the cation–cation bond length distribution; one for the host cationic species and other for the cationic dopants. It is expected that at higher Be doping levels, the second shell environment becomes more vivid comprising of both the Be and Zn atoms. For instance, the coordination occupancy of Be atom is expected to be four in comparison to the value of zinc occupancy of nine in the sample $Zn_{0.73}Be_{0.27}Se$. Hence, it is much easier to analyze first co-ordination shell around the Zn core in relation to its second atomic shell. Nevertheless, still the Zn*–Se single scattering is the main contributor to the total EXAFS intensity[15].

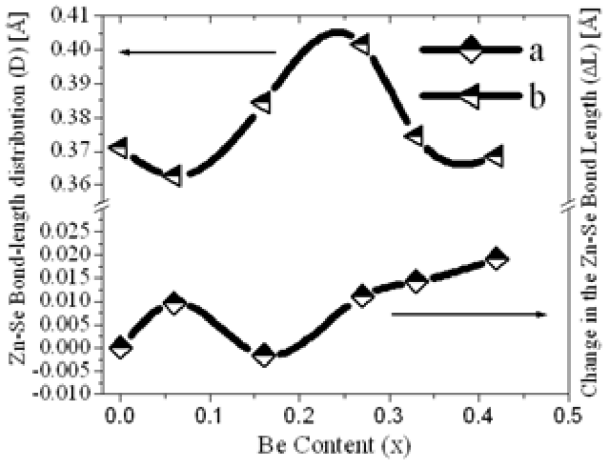

Figure 4 (a) A change in the NN distance (Zn-Se bond length) in the ternary alloy with respect to Be content (x) from the relaxes Zn-Se bond value of 2.58 Å, (b) Zn-Se Bond length distribution (D) calculated from the FWHM disorder obtained in the first Se neighbor distances of Zn core.

Amongst all the alloy compositions, we have obtained the strongest and most dependable EXAFS signals only from the scattering events for the first co-ordination shell's path (Zn*–Se). Peak position of the EXAFS Fourier transform and its full width and half maxima (FWHM) is an effective way to find the change in the bond length (ΔL) and bond disorder (D). The results of these two composition dependent variants for this alloy are shown in a figure 4. Clearly, the composition dependency in large change of the Zn–Se bond lengths on increasing the Be content in the alloy of $Zn_{1-x}Be_xSe$ system is observed. The positive values of ΔL indicate decrease in average Zn–Se bond lengths with the corresponding solid solution hardening induced by increasing the Be concentrations. The highest as-obtained value of relative bond length change is found to be 0.02 Å for the alloy composition of 42% Be-doping. The change indicates towards the increased solid solution hardening of the Zn–Se bonds and follows a general trend of decrease in ZnSe bonds and thus confirms the alloy hardening as shown in the figure 4(a). Surprisingly, during the initial stages of alloying and with the addition of Be, particularly, in the alloy sample (B) with Be content of 16% we have found the solid solution softening instead of hardening. However, the average bond variations for samples (A and C) are almost equal. Hence, initially the bond length contrasts shows a flip–flop behavior arising from the crossover in between soft–hard bond nature, which can be ascribed to ionicity induced various competing relaxations processes of structural instabilities and frustrations present in the alloy. With a careful comparison of values of the disorder (D) at different compositions, we have also found an increase of 0.05 Å in the values of EXAFS radial distributions at half maxima showing the increase of disorder with alloying in the figure 4(b). The disorder increases to a maximum value of 0.41 Å at the 27% Be concentrations from the initial value of 0.36 Å. Incredibly, the disorder decreases thereafter again to the similar value of 0.36 Å at higher Be content of 42% in the sample (E). Such an anomalous behavior indicates towards an alloying phenomenon in which the $Zn_{1-x}Be_xSe$ system first becomes fully disordered at the threshold Be concentration of 27%. This composition has the largest variations in the single Zn–Se bond length distributions with signatures of the presence of multi modal behavior of this bond. Unforeseen to this, for the concentrations of 16% to 27%, we have also found the small variations in the ZnSe bond lengths. Using these two competitive effects, we can say that the disorder in this doping state originate due to some structural relaxation induced stabilities, given by the fact that Be-Se is a harder bond. Hence, we have obtained the maximum disorder and minimum change in the respective bond lengths for this compositional state[18].

4. **Conclusion**

With the aid of modern ab initio codes, the theoretical EXAFS oscillations in various spaces are simulated and fitted with total experimental EXAFS for attaining oscillatory amplitude contributions from various single and multiple x-ray scattering paths. Significant composition dependent variations in the disorder and the single scattering path length parameter have been obtained on increasing the values of the 'x' in the range of 0.06 to 0.42 and various steps of parametric evaluation are duly accredited in the manuscript. Following the parametric extraction, we have studied the bond length distributions and relative changes in the ZnSe

bond length. Our results point in general towards the solid solution hardening of the alloy with increasing Be concentration and more specifically they describe the presence of multi modal ZnSe bond length behaviors and the presence of the structural stabilities just before the threshold concentrations

Acknowledgements

It is necessary to mention a special recognition goes to the beamline staff, synchrotron SOLEIL. They are gratefully acknowledged for their help in the EXAFS measurements under the project CEFIPRA-3204-1.

References

1. Berghout A., Zaoui A., Hugel J., Phys. Rev. B 75, 205112 (2007).
2. Plazaola F., Flyktman J. and Saarinen K., *J. of Appl. Phys 94,* 1647 (2003).
3. Pages O., Postnikov A.V. and Kassem M., Phys. Rev. B 77, 125208 (2008)
4. Tsai W.C., Cheng C.L., Chen T.T., Appl. Phys. Lett. 89, 121918 (2006).
5. Breidi A, Postnikov AV, Hassan F, Phys. Rev. B 81, 205213 (2010).
6. Ganguli T., Mazher J., *Polian A., J. Phys.: Conf. Ser. 190,* 012064 (2009).
7. Ganguli T., Mazher J., Polian A., *J. Appl. Phys. 108,* 083539 (2010).
8. Zakrzewski J., Malinski M., Pawlak M., Phys. Stat. Sol. (C) 3, 746, (2006).
9. Bukaluk A., Wronkowska A.A., Wronkowski A, Applied Surface Science 175, 531 (2001).
10. Malinski M., Chrobak L., Zakrzewski J., Opto-Electronics Review 19, 183 (2011).
11. ODE beamline (2007) URL: www.synchrotron-soleil.fr/Recherche/LignesLumiere/ODE
12. Baudelet F., Kong Q., Nataf D., J. High Pressure Research 31, 136 (2011).
13. IFEFFIT Documentation (2010) URL: http://cars9.uchicago.edu/ifeffit
14. Lee P.A., Citrin P.H., Eisenberger P., Rev. Mod. Phys. 53, 769 (1981)
15. Ravel B., Newville M., *J. of Synchrotron Radiation 12,* 537 (2005).
16. Sayers D.E., Bunker B., "X-Ray Absorption", Wiley, New York, pp 216 (1988).
17. Rehr J.J., Albers R.C., Natoli C.R., Phys. Rev. B 34, 4350 (1986)
18. Bhalerao G., Polian A., Gauthier M., *J. Appl. Phys. 108,* 083533 (2010).